Biofuel blending reduces aircraft engine particle emissions at cruise conditions

Richard H. Moore[1,*], **Kenneth L. Thornhill**[1,2], **Bernadett Weinzierl**[3,4], **Daniel Sauer**[3,4], **Eugenio D'Ascoli**[3,4], **Brian Beaton**[1], **Andreas J. Beyersdorf**[1], **Dan Bulzan**[6], **Chelsea Corr**[1,5], **Ewan Crosbie**[1,5], **Robert Martin**[1], **Dean Riddick**[1], **Michael Shook**[1,2], **Gregory Slover**[1], **Christiane Voigt**[3], **Robert White**[1], **Edward Winstead**[1,2], **Richard Yasky**[1], **Luke D. Ziemba**[1], **Anthony Brown**[7], **Hans Schlager**[3], **Bruce E. Anderson**[1]

[1]NASA Langley Research Center, Hampton, VA, USA

[2]Science Systems and Applications, Hampton, VA, USA

[3]Deutsches Zentrum für Luft- und Raumfahrt (DLR), Oberpfaffenhofen, Germany

[4]Ludwig Maximillians University, Munich, Germany

[5]NASA Postdoctoral Program, Oak Ridge, TN, USA

[6]NASA Glenn Research Center, Cleveland, OH, USA

[7]National Research Council – Canada, XXX, Canada

Abstract

Aviation aerosol emissions have a disproportionately large climatic impact because they are emitted high in the relatively pristine upper troposphere where they can form linear contrails and influence cirrus clouds. Research aircraft from NASA, DLR, and NRC Canada made airborne measurements of gaseous and aerosol composition and contrail microphysical properties behind the NASA DC-8 aircraft at cruise altitudes. The DC-8 CFM-56–2C engines burned traditional medium-sulfur Jet A fuel as well as a low-sulfur Jet A fuel and a 50:50 biofuel blend. Substantial, two-to-three-fold emissions reductions are found for both particle number and mass emissions across the range of cruise thrust operating conditions. These observations provide direct and compelling evidence for the beneficial impacts of biojet fuel blending under real-world conditions.

The global aviation sector alone contributes 3.5–4.9% of the current anthropogenic radiative forcing due to emissions of fossil fuel CO_2 as well as aerosol particles that can alter the extent and properties of cirrus clouds (1–5). Of these impacts, the largest uncertainties are associated with aviation-induced cloudiness both directly from linear, persistent contrails and indirectly from the contribution of black carbon, organic, and sulfate aerosols that may act as cloud condensation nuclei (CCN) and ice nuclei (IN) (6–9). As fuel emissions of CO_2 are expected to more than double by 2050, the future aviation forcing may increase 3–4-fold over year 2000 levels (1), or even greater when using newer methods for estimating the direct radiative impact of engine-derived black carbon emissions (10). National and

* To whom correspondence should be addressed; richard.h.moore@nasa.gov.

international regulatory and advisory bodies are exploring ways to curb these emissions, including coverage of aircraft flights originating or ending in EU airspace under the EU Emissions Trading Scheme since 2012 and the recent Advance Notice of Proposed Rulemaking by the US EPA to regulate aviation CO_2 emissions under the Clean Air Act (11–13). The International Air Transport Association (IATA) and Advisory Council for Aviation Research and Innovation in Europe (ACARE) have targeted carbon-neutral growth by 2020 and a 50–75% reduction in carbon emissions by 2050 (14, 15).

Sustainable biojet fuels are a promising route for mitigating greenhouse gas emissions and are a current investment focus in both the United States and European Union. The European Advanced Biofuels Flightpath aims to enable 2 million tons of sustainable aviation biofuels to be use by 2020. Meanwhile, the U.S. Farm-to-fly initiative targets annual production of 1 billion gallons of drop-in renewable jet fuel by 2018. However, many challenges remain before aviation biofuels are widely adopted, particularly with regard to cost and sustainability. Jet fuels are more heavily-refined than the biofuels employed for surface transportation with the latter perhaps presenting a "better biomass opportunity cost", but also a myriad of alternative energy solutions other than liquid hydrocarbon-based fuels (16,17). Biojet fuels consist of a mixture of C_9–C_{16} hydrocarbons that are formed via a two-step process. First, transesterification of plant and animal oils produces oxygenated, functionalized hydrocarbons whose low density and energy content and high freezing point make them not directly viable for aviation. Consequently, in a second step, these compounds are hydroprocessed to produce a hydrotreated ester and fatty acids (HEFA) fuel that possesses many of the properties of petroleum-derived jet fuels (?, 18). Promising plant-based feed stocks for future aviation biofuels include Jatropha, Camelina, and algae (?).

Biojet fuels promise a future aviation fuel source that is not dependent on fossilized carbon, and also possess near-zero levels of sulfur and aromatic species that are common in petroleum-based jet fuels. Previous laboratory and ground test experiments using bio-based fuels or synthetic Fischer-Tropsch fuels produced from natural gas and coal feed stocks show the absence of fuel sulfur and aromatic species significantly reduces the black carbon and sulfate particle emissions from turboprop and turbofan engines (19–22). These results are important for quantifying the impact of aviation on local air quality near airports and hint that similar reductions are likely to hold for high-altitude cruise conditions; however, the engine operating conditions on the ground (e.g., temperature, pressure, fuel flow rates, fuel/air ratio, maximum thrust) are very different than those in flight. Unless we can quantify the emissions impacts associated with these low-sulfur and low-aromatic fuels under realistic flight conditions, it will be impossible for society to understand the role biojet fuels may play in the future of aviation.

NASA, DLR – The German Aerospace Agency, and National Research Council (NRC) Canada research aircraft carried out a series of flight experiments in Spring of 2013 and 2014 to quantify the real-world impacts of biofuel blending on jet engine emissions. Flights were conducted out of the NASA Armstrong Flight Research Center (AFRC) in Palmdale, CA, with the NASA DC-8 as the source aircraft. The DC-8 has four, wing-mounted CFM56-2-C1 engines that can be fed fuel from any of four segregated fuels tanks within the wings containing either a medium- or low-sulfur Jet A fuel as well as a fuselage-mounted

auxiliary tank containing a 50:50 (v/v) blend of low-sulfur Jet A fuel and a Camelina-based HEFA biojet fuel. The medium-sulfur Jet A fuel was created by doping the the low-sulfur Jet A delivered from the refinery with a small aliquot of tetrahydrothiophene in order to increase the fuel sulfur content without changing the other fuel properties. The major difference between the HEFA fuel and traditional petroleum-based fuels is that the former possess no sulfur or aromatic species, while traditional jet fuels have aromatic contents near 18–25%. In addition to strict standards related to fuel density, viscosity, and freezing behavior that impact safety of flight, fuel aromatics are limited to below 25% in order to limit solvent deterioration of nitrile elastomers; meanwhile, a minimum aromatic content of 8% was established in order to swell the elastomer seals in the some current fuel systems (23–25). For this reason, only 50:50 blends of HEFA and petroleum-based fuels are currently certified for flight. All investigated fuels conform to flight worthiness specifications outlined by ASTM (26, 27), and detailed ACCESS fuel properties are detailed in the Supporting Online Material (SOM).

The left and right inboard DC-8 engine exhaust plumes (#2 and #3, respectively) were sampled by research aircraft flying in a trailing formation at a distance of 30–150 m behind the DC-8, which corresponds to approximate plume ages of 0.15–0.75 seconds (Figure 1a). Three different fuels and three different engine thrust conditions were investigated. The thrust conditions bracket the range of realistic flight conditions on the DC-8 flight curve, which describes the relationship between engine fuel burn (proportional to thrust) and airspeed for a given aircraft weight and cruise altitude (Figure 1d). Commercial aircraft typically fly at thrust conditions at or slightly above the Maximum Range point, which corresponds to where aircraft drag is minimized, but thrust can be operationally varied by the flight crew based on schedule and fuel burn considerations.

The use of the four-engine DC-8 is quite advantageous for in-flight engine emissions testing and overcomes sampling challenges associated with using multiple fuels and thrust conditions in dual-engine flight tests for two reasons. First, the thrust settings of the two inboard engines (#2 and #3) can be varied over the range of reasonable flight operating conditions while adjusting the outboard engines (#1 and #4) to maintain a constant airspeed. Figure 1d shows three ACCESS-2 engine thrust settings (blue points) that were set at an achievable operating speed of 0.6 Mach for the NASA and DLR chase planes. Second, we can investigate both fuels on both engines during a single flight by adjusting the valves in the fuel cross feeds in order to account for differences in engine performance that influence the engine-specific emissions indices. For example, the DC-8 left inboard engine emits more particles than the right inboard engine.

The effect of thrust changes on engine emissions of particles and, particularly water vapor, is visibly evident under contrail-forming conditions, where the plume is supersaturated with respect to liquid water, satisfying the Schmidt-Appleman criterion (28–30). Conditions encountered during ACCESS did not always warrant contrail formation, and increased ultrafine particle concentrations were measured under clear air conditions, which implies substantial ice particle scavenging of these small, nucleation-mode particles. Consequently, for the purposes of this report, we confine our analysis to the determination of engine emissions indices for clear air (i.e., non-contrail-forming) exhaust plumes only. This ensures

that the reported emissions data are not affected by contrail-processing in between the engine exhaust plane and the sampling inlet.

Particle number and mass concentrations, as well as trace gas concentrations of carbon dioxide (CO_2), carbon monoxide (CO), and nitrogen oxides (NOX), were sampled by the chase aircraft through sample inlets mounted on the crown of the DLR and NASA Falcon chase aircraft and below-wing-mounted instruments on the NRC T-33. The amount of a given species emitted per kg of fuel burn is the species emissions index (EI) and was computed as described in the SOM.

Table 1 shows the geometric mean ($\overset{\times}{\div}$ one geometric standard deviation) particle and trace gas EIs for multiple penetrations of the #3 engine exhaust plume, while it was operating at medium cruise thrust (corresponding to Maximum Range in Figure 1d). EI summary statistics for the additional thrust conditions and the #2 engine are tabulated in the SOM. Particle number EIs for the traditional petroleum-based jet fuels are on the order of 10^{14}–10^{15} kg-fuel^{-1}, with the non-volatile number EI closer to 10^{14} kg-fuel^{-1} and black carbon (BC) equivalent mass EI near 15 mg kg-fuel^{-1}. These EIs, particularly those for the non-volatile particles, fall towards the lower end of previously reported EIs from previous flight test experiments conducted during the 1990s (31–35), which is attributable to efficiency gains implemented in the relatively newer CFM56–2C engines. Sulfur doping of the low-sulfur Jet A from 22±13 ppmM to 416±37 ppmM had no discernible impact on the engine particle emissions for particle diameters exceeding 10 nm (the lowest detectable size in this study); however, it is known that changes in fuel sulfur content affect the total number EI by dramatically increasing the number of sub-5-nm-diameter particles (36). Measurements of such small particles are challenging and the results can be confounded by additional factors including the plume age and instrumental detection efficiencies (35).

We also tabulate EIs for the 50:50 blend of HEFA biojet fuel and low-sulfur Jet A in Table 1 and the SOM, which show a marked, approximately two-fold reduction in both volatile- and non-volatile number emissions as compared to the medium- and low-sulfur Jet A fuels. These dramatic emissions reductions are consistent across each of the investigated engine thrust conditions (Figure 2), although the number EI reduction is slightly less pronounced at the high engine thrust setting. Ground-based tests of low-sulfur and low-aromatic Fischer-Tropsch and HEFA fuels on the NASA DC-8 engines show a similar trend with the largest particle EI reductions observed at mid-range fuel flow rates and lower particle EI reductions observed at the highest fuel flow rates in those tests (21, 22). However, differences in engine performance characteristics (e.g., fuel-air ratio, maximum fuel flow rate, inlet temperature and pressure) between surface tests and in-flight tests preclude a direct comparison of EIs, despite a number of promising approximation methods to use ground-based data to estimate cruise emissions inventories (10, 37, 38). The greatest impact on emissions is associated with a reduction in BC-equivalent mass with the biofuel blend exhibiting emissions that are 30–40% of those seen for the traditional, petroleum-based Jet A fuels.

Measured particle size distributions help to explain the differences between number and mass (volume) EIs for the two fuels as shown in Figure 3. The pronounced decrease in both total and non-volatile particle number and volume associated with the biofuel blend is

apparent, as well as a slight shift in the mode peak diameter by 3–5 nm toward smaller sizes for the number distributions and 9–12 nm for the volume distributions. This shift appears to be caused by a greater reduction in the number of larger, soot mode aerosols, which serve as condensation nuclei for semi- and non-volatile organic species and sulfuric acid. Since gas-to-particle condensation scales with particle surface area (i.e., diameter-squared), the lower soot emissions from the biojet fuel blend suppress the condensational sink, which in turn, enhances the nucleation of new particles in a compensating manner. This competition manifests itself as the lop-sided, size-dependent number emissions reductions observed in the left panels of Figure 3.

We find that blending of traditional petroleum-based fuels with a HEFA biojet fuel significantly reduces the volatile and non-volatile particle emissions at real-world cruise conditions, with comparatively minor reductions in CO observed at one of the three engine thrust conditions. Despite these 2–3-fold emissions reductions, the soot particle number EIs remain in the range of $\sim 10^{14}$ kg-fuel^{-1}; Kärcher et al. describe this condition as squarely within the soot-rich regime, where the number of contrail ice particles scales proportionally with the soot number EI and ambient and ultra-fine particles are unlikely to contribute meaningfully to contrail formation (4). Consequently, we expect the soot particle emissions reductions form biofuel blending to translate directly into reduced contrail ice crystal density.

Understanding the implications of these findings for future aviation effects on climate is challenging due to the complex interplay between direct climatic impacts of sulfate, nitrate, and BC soot emissions and their role in forming linear contrails and contrail-induced cirrus clouds. The direct radiative impacts of sulfate and nitrate aerosols are thought to be cooling, while BC, linear contrails, and contrail cirrus are thought to be warming (1). The FAA-sponsored Aviation Climate Change Research Initiative (ACCRI) recently evaluated the direct and indirect aviation effects on climate in an ensemble modeling study (6). They assumed a cruise-altitude BC mass EI of 30 mg kg-fuel^{-1} and a number EI of 2×10^{14} kg-fuel^{-1}; these values are consistent with the observed EIs in this report for the medium-sulfur Jet A at a thrust setting between the medium and high thrust test conditions. For present-day conditions (based on year 2006 traffic data), they uncovered a weak direct global radiative forcing associated with aviation BC emissions (0.6–1.0 mW m^{-2}) and stronger radiative forcings (and greater uncertainties) associated with sulfate and nitrate (-7.0 to -14.5 mW m^{-2} combined), linear contrails (2.9–11.3 mW m^{-2}), and contrail cirrus (2.9–11.3 and 12.4–51.3 mW m^{-2}). The regional forcing for the northern hemisphere is even greater, owing to the high density of air traffic north of the equator (6). Widespread adoption of biojet fuel blends with near-zero fuel sulfur and reduced aromatic species in the future will serve to decrease the minor direct warming associated with BC and the direct cooling associated with sulfate aerosols. It remains to be seen, however, if the reduced soot EIs and expected contrail ice density reduction translate into a meaningful change in the cloud forcing or lifetime. A critical first step is the determination of the number and size of engine exhaust particles at cruise conditions, for which data are non-existent for for engines burning biojet fuel blends and sparse even for conventional, petroleum-based fuels (4). This work provides the key aerosol microphysical parameters needed by transportation and climate modeling efforts to

constrain future aviation impacts on the environment as the fleet transitions to toward widespread adoption of aviation biofuels.

Supplementary Material

Refer to Web version on PubMed Central for supplementary material.

References and Notes

1. Lee DS, et al., Atmospheric Environment 44, 4678 (2010). [PubMed: 32288556]

2. Tesche M, Achtert P, Glantz P, Noone KJ, Nature Communications 7, 12016 (2016).

3. Burkhardt U, Kärcher B, Nature Climate Change 1, 54 (2011).

4. Kärcher B, Burkhardt U, Bier A, Bock L, Ford I, Journal of Geophysical Research – Atmospheres 120 (2015).

5. Hendricks J, Kärcher B, Lohmann U, Ponater M, Geophysical Research Letters 32, L12814 (2005).

6. Brasseur GP, et al., Bulletin of the American Meteorological Society pp. 561–583 (2016).

7. Gettelman A, Chen C, Geophysical Research Letters 40, 2785 (2013).

8. Liu X, Penner JE, Wang M, Journal of Geophysical Research 114, D03204 (2009).

9. Petzold A, et al., Atmospheric Chemistry and Physics 5, 3187 (2005).

10. Stettler ME, Boies AM, Petzold A, Barrett SR, Environmental Science and Technology 47, 10397 (2013). [PubMed: 23844612]

11. EU, Directive 2008/101/EC of the European Parliament and of the Council of 19 November 2008 amending Directive 2003/87/EC so as to include aviation activities in the scheme for greenhouse gas emission allowance trading within the Community (2008).

12. US C.F.R. Vol. 80, No. 126, Proposed Finding That Greenhouse Gas Emissions From Aircraft Cause or Contribute to Air Pollution That May Reasonably Be Anticipated To Endanger Public Health and Welfare and Advance Notice of Proposed Rulemaking (2015).

13. US EPA, Fact Sheet: EPA takes first steps to address GHG emissions from aircraft engines (2015).

14. Ringbeck J, Koch V, Biofuels 1, 519 (2010).

15. Realising Europe's Vision for Aviation: Strategic Research & Innovation Agenda (Executive Summary), Tech. rep, Advisory Council for Aviation Research and Innovation in Europe (ACARE) (2012).

16. Rye L, Blakey S, Wilson C, Energy & Environmental Science 3, 17 (2010).

17. Warshay B, Pan J, Sgouridis S, Biofuels 2, 33 (2011).

18. Savage N, Nature 474, S9 (2011).

19. Corporan E, et al., Energy & fuels 21, 2615 (2007).

20. Lobo P, Hagen DE, Whitefield PD, Environmental science & technology 45, 10744 (2011). [PubMed: 22043875]

21. Beyersdorf AJ, et al., Atmospheric Chemistry and Physics 14, 11 (2014).

22. Moore RH, et al., Energy & Fuels 29, 2591 (2015).

23. Moses CA, Roets PN, Journal of Engineering for Gas Turbines and Power 131, 041502 (2009).

24. Corporan E, et al., Energy & Fuels 25, 955 (2011).

25. DeWitt MJ, Corporan E, Graham J, Minus D, Energy & Fuels 22, 2411 (2008).

26. ASTM D1655: Standard specificiation for aviation turbine fuels, ASTM International. http://www.astm.org/Standards/D1655.htm.

27. ASTM D7566: Standard specificiation for aviation turbine fuel containing synthesized hydrocarbons, ASTM International. http://www.astm.org/Standards/D7566.htm.

28. Schmidt E, Schriften det Deutschen Akademie der Luftfahrt-forschung (Oldenbourg, 1941), vol. 44, chap. Die Entstehung von Eisnebel aus den Auspuffgasen von Flugmotoren, pp. 1–22.

29. Appleman H, Bulletin of the American Meteorological Society 34, 14 (1953).

30. Schumann U, et al., Journal of Geophysical Research 101, 6853 (1996).

31. Anderson BE, et al., Geophysical Research Letters 25, 1689 (1998).

32. Schröder F, et al., Geophysical Research Letters 25, 2789 (1998).

33. Toon OB, Miake-Lye RC, Geophysical Research Letters 25, 1109 (1998).

34. Petzold A, Döpelheuer A, Brock C, Schröder F, Journal of Geophysical Research: Atmospheres (1984–2012) 104, 22171 (1999).

35. Schumann U, et al., Journal of Geophysical Research: Atmospheres (1984–2012) 107, AAC (2002).

36. Brock CA, et al., Journal of Geophysical Research 105, 26,555 (2000).

37. Petzold A, Döpelheuer A, Aerosol Science and Technology 29, 355 (1998).

38. Peck J, Oluwole OO, Wong H-W, Miake-Lye RC, Journal of the Air & Waste Management Association 63, 367 (2013). [PubMed: 23556245]

39. We thank the flight crew of the NASA DC-8. This work was supported by the NASA Advanced Air Vehicles Program, Advanced Air Transport Technology Project. RHM was supported by a NASA Postdoctoral Program fellowship.
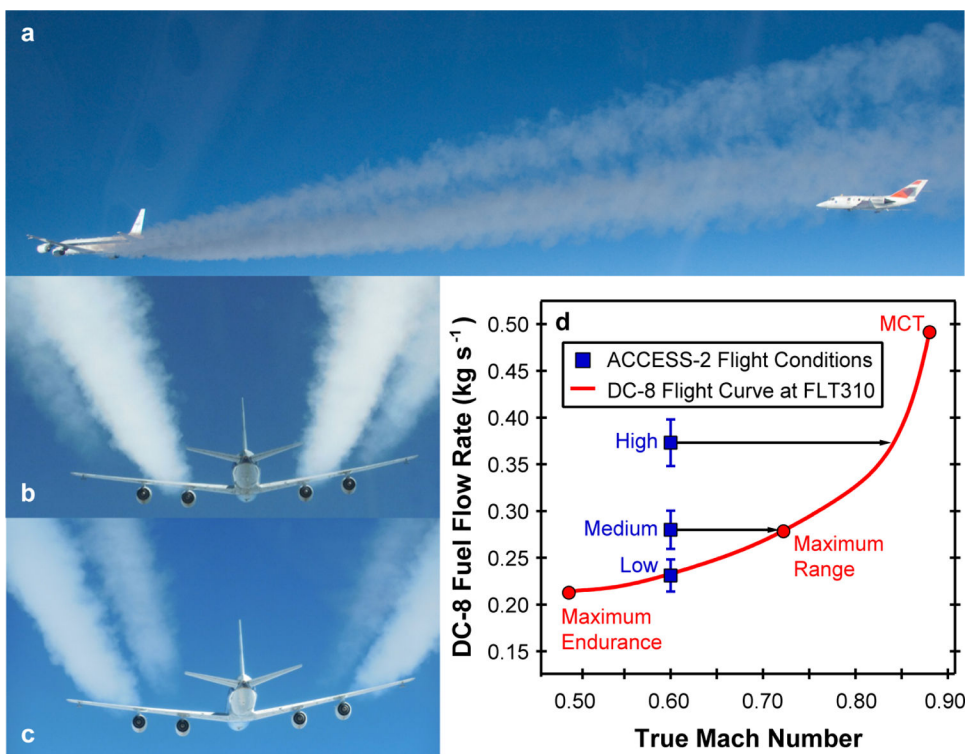
Figure 1:
Side view of the NASA HU-25 Falcon aircraft sampling the DC-8 contrail (a). Also shown are forward views of the DC-8 contrails with the inboard engines throttled up to maximum continuous thrust (MCT) and the outboard engines throttled back (b), and the reverse conditions (c). The operational flight curve for the DC-8 is shown as the red curve in (d) assuming an average aircraft gross weight of 200,000 lbs. The blue points correspond to the ACCESS-2 engine thrust settings. Note that all EIs reported in this manuscript are for clear air (i.e., non-contrail-forming conditions).
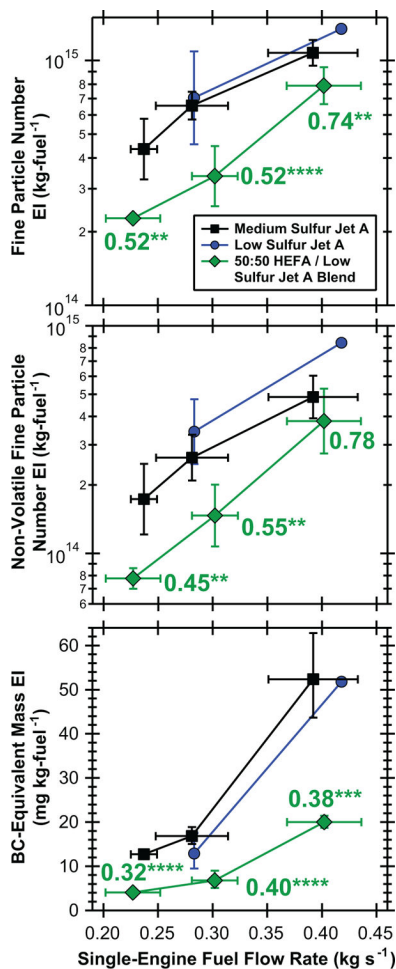
Figure 2:
Geometric mean particle emissions indices (× one geometric standard deviation) for all thrust
settings and each fuel burned on the right inboard engine (#3) at altitudes between 30,000
and 36,000 ft. The ratio of the EIs for the 50:50 biofuel blend and the medium sulfur Jet A
are denoted beside each point with the number of stars denoting the statistical significance
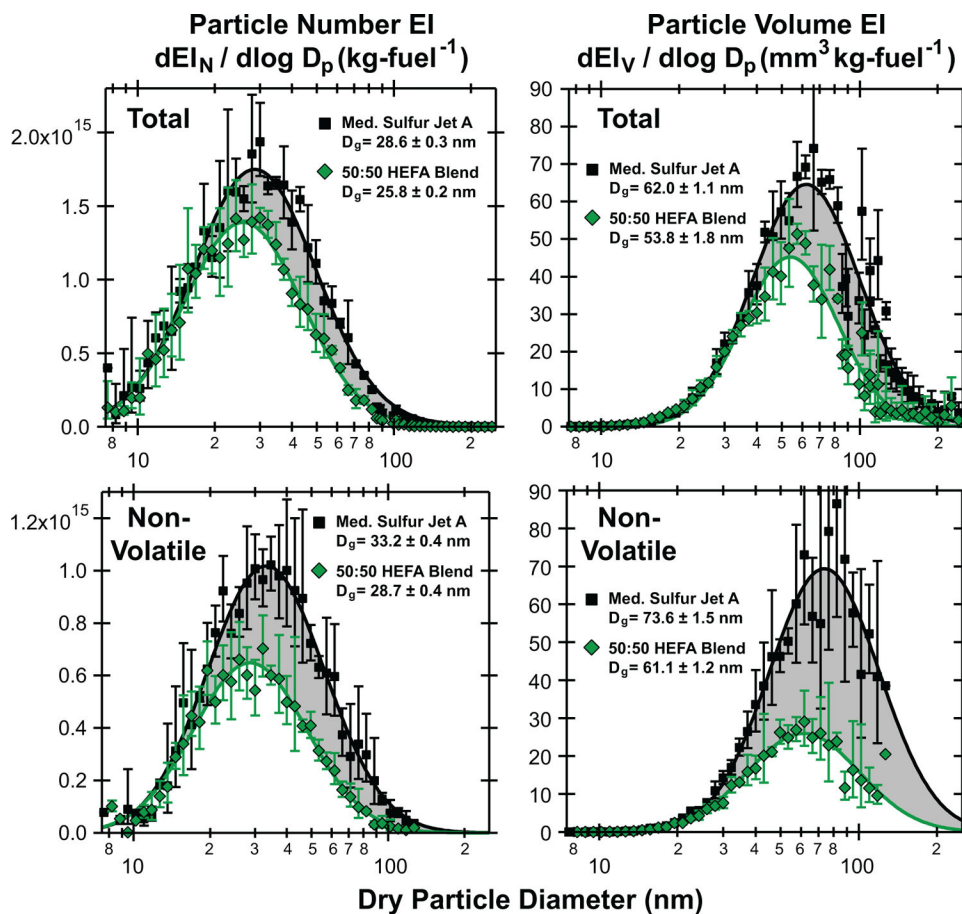level as given in Table 1 and in the SOM.

Figure 3:

Particle number (left) and volume (right) EI size distributions for the total (top) and non-volatile fraction (bottom) measured at the high thrust condition behind the #3 engine. Points are geometric means and error bars are the geometric standard deviation (N = 4 and 6 for the High Sulfur Jet A and 50:50 Low Sulfur Jet A – HEFA blend, respectively). Solid lines are lognormal fits and the shaded area represents the difference between the two curves. The geometric mean diameter for each fit are denoted in the legend, while all fit parameters are given in the SOM.

Table 1:

Summary table of emissions indices measured in clear air at the medium thrust cruise condition. Data are for the right inboard engine (#3) at altitudes between 30,000 and 36,000 ft. Data for other thrust settings are included in the SOM.

Emissions Index Parameter (per kg fuel)	Medium Sulfur Jet A — Emission Index[‡]	Low Sulfur Jet A — Emission Index[‡]	Low Sulfur Jet A — Ratio	50:50 HEFA – Low Sulfur Jet A Blend — Emission Index[‡]	50:50 HEFA – Low Sulfur Jet A Blend — Ratio
Total Particle Number ($D_p > 5$ nm)	-	$1.94 \times 10^{15} \overset{\times}{\div} 1.53$	-	$1.58 \times 10^{15} \overset{\times}{\div} 1.64$	-
Ultrafine Particle Number ($5 < D_p < 10$ nm)	-	$1.40 \times 10^{15} \overset{\times}{\div} 1.62$	-	$1.24 \times 10^{15} \overset{\times}{\div} 1.74$	-
Fine Particle Number ($D_p > 10$ nm)	$6.51 \times 10^{14} \overset{\times}{\div} 1.14$	$7.01 10^{14} \overset{\times}{\div} 1.55$	1.08	$3.36 \times 10^{14} \overset{\times}{\div} 1.33$	**0.52**[****]
Volatile Fine Particle Number	$3.86 \times 10^{14} \overset{\times}{\div} 1.08$	$3.52 \times 10^{14} \overset{\times}{\div} 1.74$	0.91	$1.86 \times 10^{14} \overset{\times}{\div} 1.38$	**0.48**[****]
Non-Volatile Fine Particle Number	$2.63 \times 10^{14} \overset{\times}{\div} 1.26$	$3.43 \times 10^{14} \overset{\times}{\div} 1.39$	1.3	$1.46 \times 10^{14} \overset{\times}{\div} 1.37$	**0.55**[**]
Total Particle Volume ($5 < D_p < 120$ nm) (mm^3)	$16.58 \overset{\times}{\div} 1.14$	$18.03 \overset{\times}{\div} 1.85$	1.09	$8.62 \overset{\times}{\div} 1.72$	0.52
Volatile Particle Volume (mm^3)	$5.62 \overset{\times}{\div} 1.67$	$5.98 \overset{\times}{\div} 1.86$	1.06	$2.90 \overset{\times}{\div} 1.88$	0.52
Non-Volatile Particle Volume (mm^3)	$10.65 \overset{\times}{\div} 1.11$	$12.03 \overset{\times}{\div} 1.85$	1.13	$5.42 \overset{\times}{\div} 1.73$	**0.51**[**]
PSAP BC-Equivalent Mass at 467 nm (mg)	$17.12 \overset{\times}{\div} 1.12$	$14.48 \overset{\times}{\div} 1.24$	0.85	$7.24 \overset{\times}{\div} 1.33$	**0.42**[****]
PSAP BC-Equivalent Mass at 530 nm (mg)	$16.85 \overset{\times}{\div} 1.12$	$12.89 \overset{\times}{\div} 1.36$	0.76	$6.79 \overset{\times}{\div} 1.33$	**0.40**[****]
PSAP BC-Equivalent Mass at 660 nm (mg)	$16.15 \overset{\times}{\div} 1.13$	$16.07 \overset{\times}{\div} 1.16$	0.99	$6.01 \overset{\times}{\div} 1.39$	**0.37**[****]
Carbon Monoxide, CO (g)	5.99 ± 0.96	4.02 ± 0.54	**0.67**[**]	4.68 ± 1.27	**0.78**[*]
Nitrogen Oxides, NO_x (g)	7.26 ± 0.50	7.60 ± 0.41	1.05	7.28 ± 0.33	1.00
Number of Plume Intercepts	4	5		10	

Significance Level:

[****] $p < 0.001$,

[***] $p < 0.01$,

[**] $p < 0.05$,

[*] $p < 0.1$

[‡] Particle EIs are reported as the geometric mean $\overset{\times}{\div}$ the geometric standard deviation, while trace gas EIs are reported as the arithmetic mean $\pm$ the arithmetic standard deviation.